Biochimica et Biophysica Acta 1859 (2017) 924–930

Contents lists available at ScienceDirect

Biochimica et Biophysica Acta

journal homepage: www.elsevier.com/locate/bbamem

Refractive index and thickness determination in Langmuir monolayers of myelin lipids

Julio M. Pusterla [a], Antonio A. Malfatti-Gasperini [b], Ximena E. Puentes-Martinez [b], Leide P. Cavalcanti [b,1], Rafael G. Oliveira [a,*]

[a] Centro de Investigaciones en Química Biológica de Córdoba (CIQUIBIC-CONICET) - Departamento de Química Biológica, Facultad de Ciencias Químicas, Universidad Nacional de Córdoba, Ciudad Universitaria, X5000HUA, Córdoba, Argentina

[b] Brazilian Synchrotron Light Laboratory - LNLS, CNPEM, Rua Giuseppe Maximo Scolfaro, 10000, Campinas, SP 13083-070, Brazil

ARTICLE INFO

Article history:
Received 10 August 2016
Received in revised form 9 February 2017
Accepted 11 February 2017
Available online 16 February 2017

Keywords:
Myelin lipids
Langmuir monolayers
Reflectivity
Thickness
Refractive index
Brewster angle microscopy
GIXOS
SAXS

ABSTRACT

Langmuir monolayers at the air/water interface are widely used as biomembrane models and for amphiphilic molecules studies in general. Under controlled intermolecular organization (lateral molecular area), surface pressure, surface potential, reflectivity (R) and other magnitudes can be precisely determined on these planar monomolecular films. However, some physical parameters such as the refractive index of the monolayer (n) still remain elusive. The refractive index is very relevant because (in combination with R) it allows for the determination of the thickness of the film. The uncertainties of n determine important errors that propagate non-linearly into the calculation of monolayers thickness.

Here we present an analytical method for the determination of n in monolayers based on refractive index matching. By using a Brewster angle microscopy (*BAM*) setup and monolayers spread over subphases with variable refractive index (n_2), a minimum in R is search as a function of n_2. In these conditions, n equals n_2. The results shown correspond to monolayers of myelin lipids. The n values remain constant at 1.46 upon compression and equals the obtained value for myelin lipid bilayers in suspension. The values for n and R allow for the determination of thickness. We establish comparisons between these thicknesses for the monolayer and those obtained from two X-ray scattering techniques: 1) *GIXOS* for monolayers at the air/water interface and 2) *SAXS* for bilayers in bulk suspension. This allows us to conclude that the thickness that we measure by *BAM* includes the apolar and polar headgroup regions of the monolayer.

1. Introduction

Langmuir monolayers of amphiphilic lipids constitute a convenient experimental system to model biomembranes [1]. A big variety of physical parameters can be easily and precisely determined on these planar monomolecular films, such as surface pressure, molecular area, surface potential and others [2]. This is in part due to the macroscopically planar nature of the film. In the optical domain, reflectivity (R) can be measured with Brewster angle microscopes (*BAM*) [3] even with very simple setups [4]. Although some progress has been achieved [5,6] the refractive index of the floating monolayer (n) still remains an elusive parameter [1]. Both in conjunction, n and R are very relevant because a precise knowledge of them allows for the calculation of the thickness of the film in situ, for instance on a *BAM* [7]. They can be in principle modeled by ellipsometric angles determination, but the technical implementation of ellipsometry at the air/water interface is not a standard technique [8,9], being difficult due to the very thin nature of the layer and the low contrast in refractive index between the water and the film, typically between 1.4 and 1.5. Ellipsometry at the air/water interface is even more difficult if there are lipid domains (an active field of research) due to the movement of the film and the time required to make a measurement.

In order to overcome these limitations, a common practice is to assume a value of n that can be fixed, even for different lipids [10,11], or allowed to vary in a range [12–14] at the expense of accuracy in thickness that can be enough for some simple purposes, like ensuring the monomolecular nature of the film or checking the increment on global thickness upon compression or adsorption [13,15]. Nevertheless, care should be taken in not over-interpreting results. An error in the value of n propagates non-linearly into thickness errors. These errors can become unacceptable big for more detailed studies, which normally require X-ray scattering techniques [16,17].

Abbreviations: *BAM*, Brewster angle microscopy; *CNS*, central nervous system; *DPPC*, 1,2-dipalmitoyl-sn-glycero-3-phosphocholine; *SAXS*, small angle X-ray scattering; *GIXOS*, grazing-incidence X-ray scattering out of the specular plane; *XRD*, X-ray diffraction.

* Corresponding author at: Centro de Investigaciones en Química Biológica de Córdoba, CIQUIBIC, CONICET, X5000HUA Córdoba, Argentina.
E-mail address: oliveira@fcq.unc.edu.ar (R.G. Oliveira).
[1] Current address: School of Chemical Engineering, University of Campinas, Brazil.

http://dx.doi.org/10.1016/j.bbamem.2017.02.005
0005-2736/

Here we present an analytical method for the experimental determination of n in optically isotropic fluid monolayers based on the principle of refractive index matching as used in bulk suspensions of liposomes [18] and nanoparticles [19], but adapted to Langmuir monolayers. By using a *BAM* setup [3,20] and monolayers spread over subphases with different and known refractive index n_2, a minimum in reflectivity is search as a function of the refractive index of the subphase. When this condition is met, the (unknown) refractive index of the monolayer n equals the known refractive index of the subphase n_2.

Here we choose for our studies the lipidic fraction of the myelin membrane [21], which account for 75–80% of the whole membrane, the major percentage known for any membrane. Myelin (and its lipid fraction) is a biophysically interesting material [22,23] that can be spread at the air/water interface as monolayers and remain as one of the best characterized natural membranes by Langmuir trough studies [24]. Additionally, it is one of the easiest and best characterized membranes by use of X-ray and neutron scattering and diffraction [15,25,26]. This conforms a set of background data available from different techniques, which is not common to find for other ultrathin natural biosystems. Nevertheless, the method developed is of general application in the field of amphiphilic molecules.

2. Materials and methods

2.1. Myelin lipid purification and monolayer preparation

Highly purified myelin was prepared from bovine spinal cord [27]. For isolation of total myelin lipid extract, the lower solvent phase of a Folch's partition [28] of the previously purified myelin was equilibrated (in proportion 1:1) with a chloroform–methanol–water (3:48:47) solution saturated with potassium citrate (0.1 M). In this condition, the Folch's proteolipid becomes insoluble and can be removed because it accumulates at the two-solvent interface [29]. The procedure is repeated three times. Subsequently, the lower phase is washed with a citrate-free upper phase (in proportion 1:1). The myelin lipid extract is mainly composed by cholesterol (0.38), phosphatidylethanolamine (0.19), cerebroside (0.15), sphingomyelin (0.08), phosphatidylcholine (0.06), phosphatidylserine (0.05) and sulfatide (0.04) in mole fraction [21]. The lipids are spread directly at the air/aqueous interface from the resulting solution [30]. Typical error in surface pressure is ± 1 mN/m.

2.2. Brewster angle microscopy

An EP3 single wavelength ellipsometer from Accurion (Göttingen) with an antivibration system (Vario 40-100) from the same manufacturer was used in *BAM* setup, i.e. light polarized in the plane (p) of incidence, from a laser of 532 nm wavelength (50 mW) at the Brewster angle. A Langmuir minitrough (KSV, Helsinki) via Wilhelmy plate was mounted on top of the ellipsometer stage. For compression isotherms the minitrough was used and spreading was up to below 1 mN/m. For reflectivity measurements of the p component (R_p) a smaller trough was used and the lipid was spread up to the target surface pressure. Reflectivity is measured after imaging acquisition via CCD and proper calibration of gray level vs R_p [15]. This allows to measure R_p even in heterogeneous monolayers at specific regions of interest (domains).

2.3. Aqueous subphases with defined refractive index

A series of solutions of increasing concentration was prepared for glycerol and sucrose (Analytical degree). These solutions have known refractive index from the literature. In order to discard any problem related to the particular wavelength used in the bibliography, we measured the refractive index at 532 nm (wavelength of our *BAM* laser) of all the solutions by looking for the Brewster angle θ_B (Fig. S1, see Supplementary Information). Then we calculate the refractive index of the subphase n_2 from the angle according to Brewster law:

$$n_2 = \tan\theta_B \tag{1}$$

For determinations of the minima in R_p as a function of the incident angle (θ), we used routines provided by the manufacturer [15].

2.4. Determination of refractive index

Langmuir monolayers were spread over different subphases and analyzed at the corresponding Brewster angle of each subphase. This allows us to determine the refractive index of the monolayer itself. This is done by looking for the subphase that minimizes the reflectivity from the monolayer (that is to make the monolayer virtually invisible) according to the principle of refractive index matching usually used in suspensions.

2.5. Determination of thickness of monolayer

By knowing the refractive index of the lipid monolayer for all surface pressure values, we calculate the film thickness. The gray level of each section of the micrographs was then converted to reflected light intensity (R_p), and the thickness (l) was calculated assuming a smooth but thin interface in which the refractive index varies along the normal of the interface on a distance l, much smaller than the incident light wavelength [7,15], giving:

$$l = \frac{\sqrt{R_p}}{\sin(2\theta_B - 90)} \left(\frac{\pi \sqrt{n_1^2 + n_2^2}(n_1^2 - n^2) \times (n_2^2 - n^2)}{\lambda (n_1^2 - n_2^2) n^2} \right)^{-1} \tag{2}$$

2.6. Measurements of refractive index of membranes in bulk suspensions

The same series of glycerol/water solutions used as subphase for monolayer studies were also employed as bulk suspension liquid media for determination of refractive index of bilayers. Myelin lipid fraction was suspended at 1.50 mg/ml in this solution series. A UV-2401PC spectrophotometer (Shimadzu, Japan) operating at 532 nm (the same wavelength of the laser in our *BAM* setup) was used to detect the minima in absorbance along the solution series of increasing refractive index. According to refractive index matching principle, the sample with best match should produce lower absorbance.

2.7. SAXS and electron density profile of unilamellar vesicles

The *SAXS* measurements were performed at the *D02A:SAXS2*beamline (Brazilian Synchrotron Light Laboratory – LNLS, Campinas, Brazil). Myelin lipids were suspended in Hepes 5 mM, pH 7.4 at 5 mg/ml at 45 °C to ensure hydration, and filled into the sample holder between two mica plates. Measurements were from 6 to 30 °C with 0.1488 nm radiation and the nominal sample detector distance was 1 m. A two dimensional MARCCD detector was used and for radial integration of the signal, we employed the free software Fit2D V12.077 from Andy Hammersley at the European Synchrotron Radiation Facility – ESRF (Grenoble, France) after background subtraction. A three-layer model was employed to fit the signal and generate the electron density profile.

2.8. GIXOS and thickness of monolayers

We are currently developing a new setup for *GIXOS* at the *D10B:XRD-2* beamline at LNLS, analogous to one previously used [17,31]. Briefly, the synchrotron horizontal beam ($\lambda = 0.154$ nm) is vertically deflected at a grazing angle (nominal 0.12°) below the critical angle for total external reflection for water (0.15°) by employing a Cr coated quartz

mirror specially designed, similar to [32] and directed toward a Langmuir trough (details to be published elsewhere). We validated the setup by comparing the minima that we obtained from a standard phospholipid (*DPPC*) with previously published data of *GIXOS*, as well x-ray reflectivity [33]. The three q positions (where q is the scattering vector) of the minima are coincident, then *GIXOS* renders equivalent information to X-ray reflectivity, and our setup is valid for this purpose. The thickness of the film (from the acyl chain/air interface to the maximum of electron density) is directly calculated from the position of the minima in specular reflectivity or *GIXOS* signals (Eq. (9)) [34].

3. Theory

For a Fresnel interface, in which the refractive index changes abruptly at the level z = 0 from n_1, the refractive index of the incidence medium to n_2, the refractive index of the second medium, the reflectivity is given by the Fresnel formulas:

$$R_s^F = \left(\frac{\sin(\theta_i - \theta_r)}{\sin(\theta_i + \theta_r)}\right)^2 \tag{3}$$

$$R_p^F = \left(\frac{\tan(\theta_i - \theta_r)}{\tan(\theta_i + \theta_r)}\right)^2 \tag{4}$$

where θ_i and θ_r are the incident and refracted angles, respectively, R_p^F is the reflectivity for p-polarized incident beam and R_s^F is the reflectivity for s-polarized incident beam.

R_s^F increases from $[(n_2 - n_1) / (n_2 + n_1)]^2$ to 1 with the angle of incidence, and R_p^F initially decreases to 0 and then increased to 1. R_p^F vanishes at an angle of incidence θ_B called the Brewster angle.

For real interfaces, such as a lipid monolayer, R_p decreases to a minimum value, but does not vanish. The origin of this discrepancy is the structure of the interface, which can be thick, rough or optically anisotropic [7]. When the thickness (l) of the interfacial region is smaller than the wavelength (λ) of the incident beam ($l \ll \lambda$) and there is also no anisotropy, optical properties of the real interfaces can be characterized by a number, the ellipticity (ρ). The Drude approach can be applied to calculate ellipticity ρ for a homogeneous interfacial film of refractive index n and thickness l:

$$\rho = \frac{l \times \pi}{\lambda} \times \frac{\sqrt{n_1^2 + n_2^2}}{n_1^2 - n_2^2} \times \frac{(n_1^2 - n^2) \times (n_2^2 - n^2)}{n^2} \tag{5}$$

In the vicinity of the Brewster angle, and if $\rho \ll 1$, the experimental R_p differs from the ideal R_p^F according to the equation:

$$R_p = R_p^F + R_s^F \times \rho^2 \tag{6}$$

At the Brewster angle, $\theta_i + \theta_r = \pi/2$ and therefore R_p^F vanishes (Eq. (4)). R_s^F can be expressed as:

$$R_s^F = \left(\frac{n_2^2 - n_1^2}{n_2^2 + n_1^2}\right)^2 \tag{7}$$

By combining Eqs. (5), (6) and (7) and fixing n_1 as 1, the reflectivity R_p at the Brewster angle is:

$$R_p(n_2) = \frac{a n_2^4 - b n_2^2 + c}{d n_2^2 + e} \tag{8}$$

In Eq. (8), $a = \boldsymbol{n}^4 - 2\boldsymbol{n}^2\boldsymbol{n}_1^2 + \boldsymbol{n}_1^4$, $b = 2\boldsymbol{n}^6 - 4\boldsymbol{n}^4\boldsymbol{n}_1^2 + 2\boldsymbol{n}^2\boldsymbol{n}_1^4$, $c = \boldsymbol{n}^8 - 2\boldsymbol{n}^6\boldsymbol{n}_1^2 + \boldsymbol{n}^4\boldsymbol{n}_1^4$, $d = \boldsymbol{n}^4$ and $e = \boldsymbol{n}^4\boldsymbol{n}_1^2$.

In the vicinity of the Brewster angle this can be approximated by a parabola.

4. Results and discussion

4.1. Refractive index on monolayers

As it is known, the Brewster angle of subphase does not change detectably after a monolayer is spread on it, but the R_p (R polarized in the specular plane) increases markedly. This increment depends on the difference of the refractive index of the monolayer (n) and the subphase (n_2), that is the contrast. The subphase refractive index was modified by making glycerol/water and sucrose/water solutions of increasing concentration.

By changing the n_2 we manipulate the contrast up to minimize it, at the point where n_2 operationally best matches n; then R_p is at a minimum, but does not vanish. This not vanishing behavior is due to the differences in refractive index between the regions (mainly hydrophobic and headgroup) of the Langmuir monolayer. This difference cannot be suppressed by any manipulation. Therefore, our effective (or global) refractive index has contributions that cannot be split by the present method, and a global refractive index for the whole monolayer is obtained [12]. We checked that the contribution of anisotropy [35] and roughness does not account for the non-vanishing behavior of R_p.

R_p as a function of n_2 is shown in Fig. 1A for a particular surface pressure (45 mN/m). The points were fitted according to Eq. (8), therefore the minimum corresponds to n, the refractive index of the monolayer.

Measurements of R_p performed at different surface pressures on glycerol/water solutions between 5 and 45 mN/m are displayed in Fig. 1B. The increment of surface pressure leads to higher R_p values

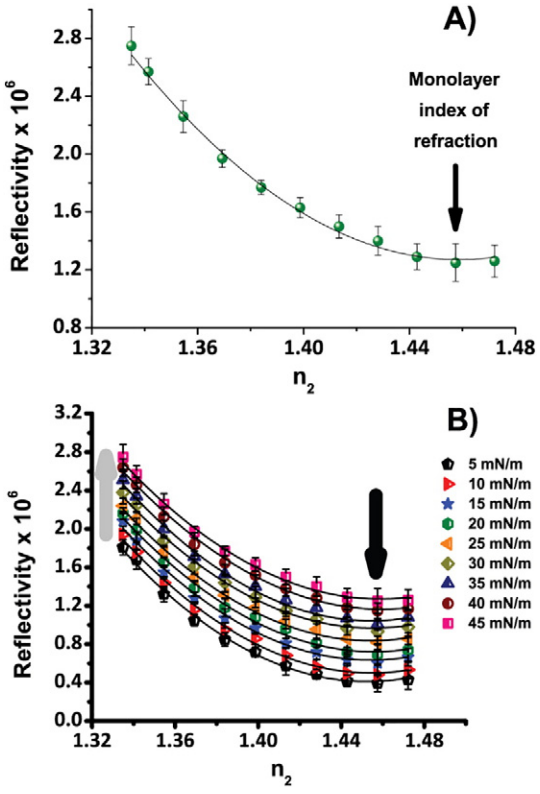

Fig. 1. Reflectivity (R_p) of myelin lipid monolayers on glycerol/water solutions with different n_2. A) Example at 45 mN/m. The n_2 of each solution was calculated from its Brewster angle and the errors correspond to the standard deviation of 3 independent determinations of the reflectivity. The solid line represents the fitting according to Eq. (8). The minima in R_p (black arrow) indicate the n of the monolayer at 45 mN/m. B) Reflectivity (R_p) of myelin lipid fraction monolayers as a function of subphase refractive index (n_2) as in A, but at different surface pressures over the range 5–45 mN/m. Solid lines are fittings as in A. The minima in R_p (black arrow) indicate that the n of the monolayer remains constant at 1.46 over all the packing conditions. A systematic increment on R_p is observed upon lateral compression (gray arrow).

(this is an effect of the increased thickness of the film upon compression), but in all cases the curves are similar parabolas and locally parallel, with the minima at the same *n* value. The values of *n* obtained from fittings does not show a significant change when the surface pressure increases (Fig. 1B). The same results are obtained when the spreading is on sucrose/water solutions (Fig. S2). The values of *n* as a function of surface pressure for both glycerol and sucrose aqueous solutions are displayed on Fig. S3. None of the films showed anisotropy (Fig. S4).

To evaluate an eventual effect over the surface behavior (attainable molecular packing and surface pressures) derived from the presence of sucrose and glycerol, comparative isotherms were performed using water, water saturated with sucrose and pure glycerol as subphases (Fig. S5), as well as intermediate concentrations (not shown). With respect to the previously reported isotherm of myelin lipid fraction on water, sucrose does not have any effect on the compression behavior (characteristic of a liquid-expanded state), with a collapse pressure of 45 mN/m and a limiting molecular area of 0.41 nm^2. When glycerol is used as subphase the compression isotherm is slightly altered, but the molecular areas attainable are in the same range as on water. As shown below, since *n* remains constant with variations of molecular area this variation does not have any effect on the determination of *n*.

4.2. Refractive index in bilayers

In order to establish a comparison with myelin lipid bilayers in bulk suspension, we applied the same contrast matching principle to suspension of vesicles in the same solutions with variable n_s (solvent refractive index) as described above [18] and we found a minimum in absorbance (due to diminished Rayleigh scattering) which is due to the matching condition at $n_s = 1.46 \pm 0.01$ (Fig. 2), which indicates an equivalence in monolayer-bilayer systems in this regard. The absorbance does not vanish for analogous reasons to the case of the monolayer.

4.3. BAM thickness on monolayers

From the constant *n* value for monolayers and the variable R_p value on water (first vertical data set, gray arrow in Fig. 1B) we calculated the monolayer global thickness (using Eq. (2)) as a function of surface pressure, which increases, as happens normally with monolayers of lipids in liquid-expanded state. In this sense, the monolayer behaves quite analogously to the observed behavior with X-ray reflectivity, that is, the optical property, electron density in X-rays [36], *n* in our optical setup, remains constant (provided no phase transition takes place) and the monolayer reacts to lateral compression increasing the thickness. According to the literature [37,38] the equivalent lateral packing between monolayers and bilayers occurs at 35–45 mN/m. At 40 mN/m the thickness is 2.50 ± 0.06 nm, going to higher surface pressure (45 mN/m) the thickness increases up to 2.55 ± 0.08 nm. We will put these values in the context of myelin membranes in the next section. Before, it should be noticed that when dealing with monolayers and membranes thicknesses, different definitions arises naturally [39]. Therefore, when measuring this property, it should be clear what parts of the supramolecular ensemble are actually measured. As noted before, this is even more problematic when using optical techniques in the visible domain [6]. Is just the hydrophobic region actually measured as sometimes assumed [10], or is the polar headgroup included? If it is included, up to what point is included? Up to maximum density in the headgroup, as in some X-ray scattering determinations? [34,39] It includes the tails due to roughness? In order to answer these important questions, we measured the myelin lipids using two different synchrotron X-ray based techniques that avoid these ambiguities (Fig. 3).

4.4. X-ray scattering techniques

4.4.1. Grazing incidence X-ray off specular scattering (GIXOS)

First, we measured the *GIXOS* of myelin lipid monolayers at different surface pressures (Fig. 4). From the *GIXOS* minima, we calculated the monolayer thickness from the air/water interface up to the maximum in the electron density profile at the headgroup [34], which goes from 1.80 nm (10 mN/m) up to 2.13 nm, at 45 mN/m. This is an unambiguous measurement which shows values 0.4 nm lower than the *BAM* results at equal surface pressure. It should be noticed that even for simple molecules like fatty acids, thickness from the visible spectra by ellipsometry and X-ray reflectivity (analogous to *GIXOS*) does not match perfectly, and differences of about 10% have been reported [6] which are related to the differential sensing of the sub-monolayer structures by the particular technique (see next section). The 2.13 nm is very consistent with the analogous maximum electron density peak position of bilayers (2.30 nm), as described in the next section.

4.4.2. Small angle X-ray scattering (SAXS)

Second, and approaching a more biologically relevant condition, we measured *SAXS* of myelin lipids in unilamellar vesicles in bulk suspension in water and modeled the signal (Fig. 5 and Table 1).

The Fig. 6 shows the modeled electron density profile of a full bilayer. We got the headgroup peak (maximum electron density) at 2.30 nm from the bilayer center, which equals the one obtained by classical X-ray diffraction experiments on myelin lipids [40].

Fig. 6 includes the maximum *BAM* and *GIXOS* thicknesses at 45 mN/m, a packing condition close to the one postulated to exist in the bilayer

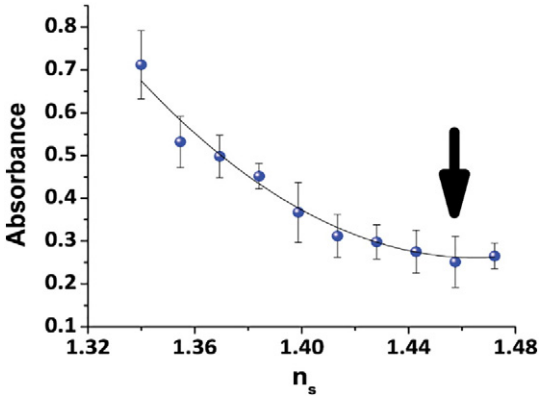

Fig. 2. Absorbance at 532 nm of myelin lipid bilayers in glycerol solutions of increasing concentration. The absorbance gets lower as the refractive index match point approaches. The fitting was performed with a parabolic function and the errors correspond to the standard deviation of 3 independent determinations of the absorbance. The resulting refractive index is 1.46 ± 0.01.

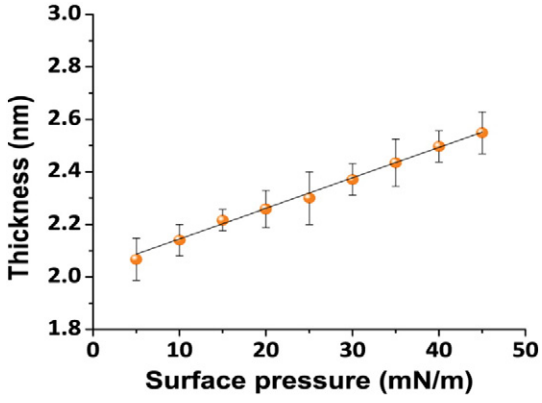

Fig. 3. Myelin lipid monolayer thickness as a function of surface pressure. The thickness was calculated from Eq. (2) using the constant refractive index ($n = 1.46$) and the variable R_p values obtained on water. It increases linearly with the compression from about 2.0 nm (extrapolated to 0 mN/m) up to values close to the ones consistent with the reported from x-ray diffraction in the literature [40].

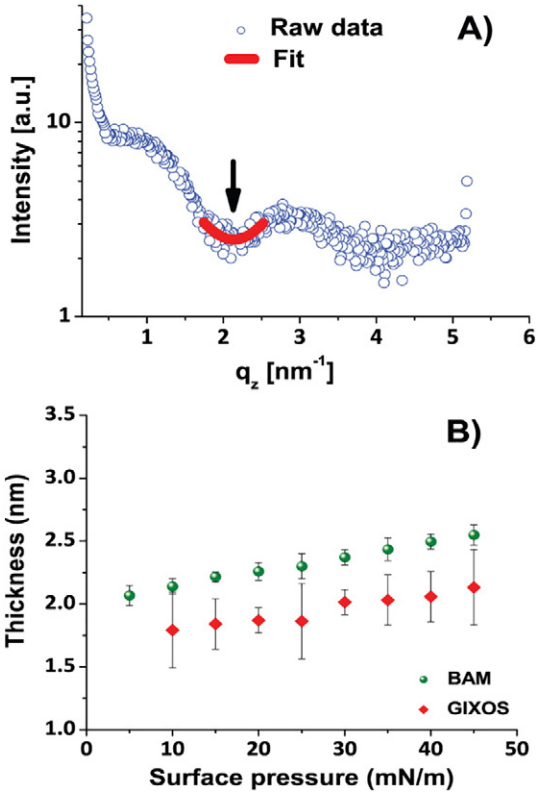

Fig. 4. *GIXOS* of myelin lipid monolayers. A) Representative *GIXOS* of myelin lipids taken at 40 mN/m. The fitting of the local minima (red full line) allows the direct determination of the thickness of the monolayer up to the maximum in electron density (phosphate groups). From the minima position (black arrow) the thickness is calculated through Eq. (9). B) Comparison of *BAM* thickness versus *GIXOS* thickness as a function of surface pressure, both grow linearly with compression. The *BAM* thickness is bigger by 0.4 nm independently of surface pressure.

(equivalent to 35–45 mN/m). As can be seen, the conjunction of *SAXS* data in bilayers and *GIXOS* in Langmuir monolayers allows a better definition of the measured "thickness" by *BAM*, which not only includes the hydrophobic part, but also the headgroup. As a conclusion *BAM* is sensitive to the monolayer as a whole. This fact agrees with previous works performed in similar experimental setups [5,6] and numerical estimations [41].

If we define the monolayer thickness as the sum of the hydrocarbon portions and the headgroup thicknesses, the average size for half of the bilayer obtained from *SAXS* data becomes approximately 2.85 nm

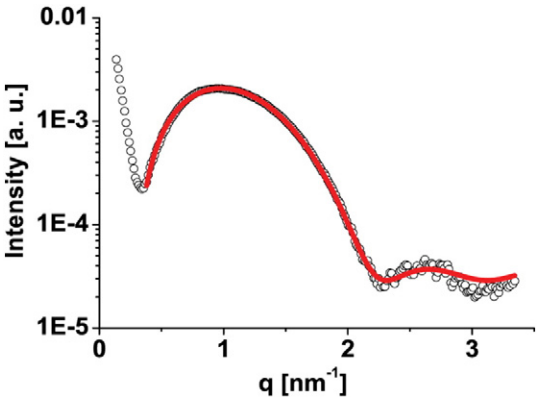

Fig. 5. *SAXS* of myelin lipids unilamellar vesicles. The signal (open circles) was fitted (red curve) using a three-layer model that generated an electron density profile of the membrane (see Fig. 6).

Table 1
Parameters of the SAXS data fitting (Fig. 5) that generates the bilayer model (Fig. 6).

	Methyl depth	Acyl chains	Headgroup
Electron density [$e^-/Å^3$]	0.156	0.316	0.352
Thickness [nm]	0.35	1.40	1.10

(Fig. 6, in green) – i.e., 0.55 nm larger than the value taken for the headgroup position from bilayer center. Finally, concerning the *GIXOS* analysis, the equation of Kjaer [34] relates the minimum in the *GIXOS* scattering pattern (q_z) with the central position of the headgroup region:

$$q_z \cong \frac{3\pi}{2} / \left(l_T + \frac{1}{2} l_H \right) \tag{9}$$

with l_T being the thickness of the hydrocarbon tail and l_H the thickness of the headgroup region.

Then to obtain the whole monolayer thickness from *GIXOS* data is necessary to sum half of the headgroup layer thickness. If we consider similar values for the headgroup layers obtained from *SAXS* and *GIXOS*, we should expect an increase in the *GIXOS* monolayer thickness of 0.55 nm (considering to be the same as *SAXS*), giving the final value of 2.68 nm, which is very close to the thickness obtained from *BAM*. Still the *GIXOS* thickness (2.13 nm) is 0.17 nm shorter than the equivalent *SAXS* thickness based on the maximum electron density peak (2.3 nm). We speculate that this is due to the fact that the mathematical superposition of the electron density profiles of the two opposing monolayers will eliminate the methyl depth, which is physically unrealistic (Fig. 7A). This is due to the different representation of bilayers (3-box models) versus monolayers (two box models), where the methyl depth is included in the roughness (0.2–0.3 nm) of the hydrocarbon/air interface. In order to reconstruct a methyl deep, the two opposing monolayers should be translated a little apart (0.15–0.2 nm) from each other (Fig. 7B) along the Z axes of Fig. 6. This is due to the fact that the rough interfaces cannot be fully superimposed. Nevertheless, as a word of caution, the discussion on the use of one-layer, two-layer and three-layer models is not trivial. The election of a proper model depends partly on the amount of raw data available in the measurement set. The reflection of different stratified layers on a support is not a linear phenomenon. The thicknesses obtained when applying one-layer (*BAM*) or two-layer models (*GIXOS*) do not coincide. This is surely one of the reasons for the discrepancies obtained when the X-ray data results and those from *BAM* are compared.

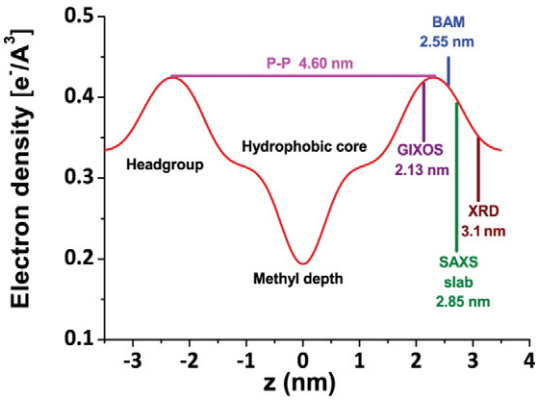

Fig. 6. Electron density profile of the myelin lipid bilayer from *SAXS* data. The 4.6 nm equals the value accepted from classical X-ray diffraction [40]. Thickness measurements from other techniques are shown by vertical lines. *GIXOS* (purple line) renders, as expected, a value quite similar to the one of the maximum in the profile. The *BAM* setup (blue line) renders values shifted to the box model, without including roughness, which thickens even more the layer (green line). As a reference, the spacing of multilamellar stack of myelin lipids from X-ray diffraction (*XRD*) is presented (brown line).

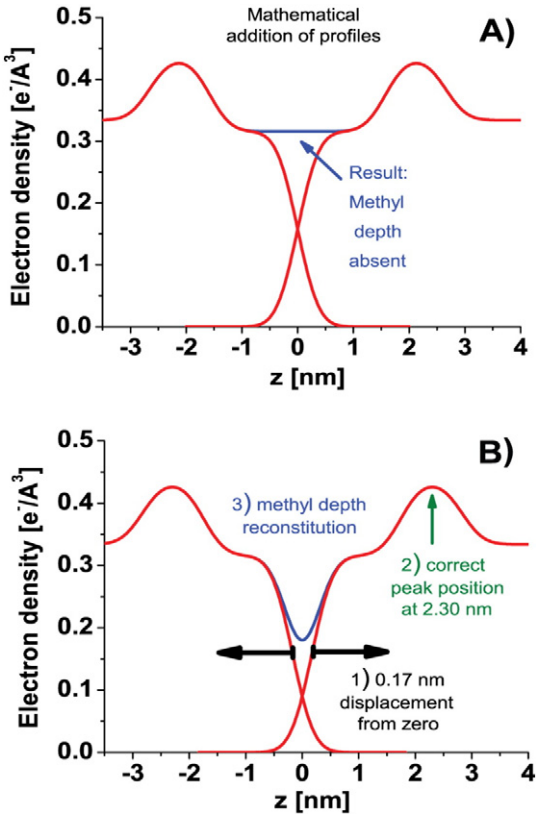

Fig. 7. Reconstruction of the e^- density profile of a bilayer from the e^- density profiles of two monolayers. In A) the mathematical addition of two opposing monolayers results (by symmetrical considerations) in a region of constant e^- density, eliminating the methyl deep. In B) the methyl deep is recovered by displacing each profile by 0.17 nm from the zero z position. 2.13 nm (*GIXOS* thickness) plus 0.17 nm of steric repulsion needed for methyl deep preservation recreates the 2.30 nm *SAXS* thickness.

Our election of myelin lipids is based on the fact that no other membrane is so heavily composed by lipids. Then studying this fraction, a good insight on the native membrane can be obtained. Besides that, for myelin related materials there are some approximations of n (although at poorly defined wavelengths). As a starting point *DPPC* in dry state has a refractive index $n = 1.478 \pm 0.006$ [42] and the cholesterol $n = 1.47 \pm 0.06$ [12]. White matter has a reported n of 1.467 ± 0.002 [43], Wendell-Smith and Williams, estimated a value of 1.48 for whole myelin, including its proteins [44]. Min used 1.47 for a reconstituted system mimicking myelin lipids [22]. With all this, our results, measured in situ in the monolayer appear as good estimates in comparison to the uncertainty on the values reported in the literature.

5. Conclusions

As stated before, having n and R_p allows the direct calculation of the thickness in situ. This information is also available from other complex techniques (ellipsometry, X-ray and neutron reflectivity, *GIXOS*). In comparison to these techniques, the method by *BAM* has the advantage that a simpler in lab setup is enough and it avoids the complications of modeling. Moreover, due to the imaging capabilities of the *BAM* the information is local and heterogeneous systems are analyzable, in contrast to the above mentioned techniques, which averages over big footprint beams. An additional advantage of refractive index matching is that can be performed in bulk suspension of liposomes, and this allows the comparison of monolayers on one side, with bilayers or multilayers in the other. It has the disadvantage that multiple monolayers and measurements are necessary. Additionally, here we show that even changing the molecular packing along the compression isotherm, the refractive index remains the same at the third digit, at least for the isotropic film analyzed. The measured thickness includes the whole film (hydrocarbon and polar headgroup) which increases linearly with surface pressure.

Our value of n for myelin lipids is close to previously existing data for related systems. The thickness derived is compatible with previous and new data. This technique will be applicable to other liquid-expanded films.

Transparency document

The Transparency document associated with this article can be found, in the online version.

Acknowledgements

This work was supported by grants from CONICET (PIP 2012-14 #11220110100624), SECyT (2014-2015 203/14) (UNC), FonCyT (PICT 2012-2583) and CeBEM (09-2012) (Argentina). We acknowledge to the Brazilian Synchrotron Light Laboratory for beamtimes at *SAXS*-2 beamline under research proposals *SAXS*1-10716 and *SAXS*1-13462 and *XRD-2*, proposal 20150072. R.G.O. thanks to FAPESP for the program of visiting researcher (grant number 14/18526-1). J.M.P. is a doctoral fellow from CONICET. R.G.O. is member of the Scientific Research Career (CIC) from CONICET. A.A.M.G. was a postdoctoral fellow from FAPESP (grant number 11/19952-6) now is part of the staff of LNLS.

Appendix A. Supplementary data

Supplementary data to this article can be found online at http://dx.doi.org/10.1016/j.bbamem.2017.02.005.

References

[1] H. Möhwald, in: R. Lipowsky, E. Sackmann (Eds.), Phospholipid Monolayers, Handbook of Biological Physics, vol. 1, Elsevier Science B.V., Netherlands 1995, pp. 163–202.
[2] P. Dynarowicz-Latka, A. Dhanabalan, O.N. Oliveira Jr., Modern physicochemical research on Langmuir monolayers, Adv. Colloid Interf. Sci. 91 (2001) 221–293.
[3] D. Hönig, D. Möbius, Direct visualization of monolayers at the air-water interface by Brewster angle microscopy, J. Phys. Chem. 95 (1991) 4590–4592.
[4] C.M. Rosetti, R.G. Oliveira, B. Maggio, Reflectance and topography of glycosphingolipid monolayers at the air-water interface, Langmuir 19 (2003) 377–384.
[5] J.G. Petrov, T. Pfohl, H. Möhwald, Ellipsometric chain length dependence of fatty acid Langmuir monolayers. A heads-and-tails model, J. Phys. Chem. B 103 (1999) 3417–3424.
[6] D. Ducharme, A. Tessier, S.C. Russev, Simultaneous thickness and refractive index determination of monolayers deposited on an aqueous subphase by null ellipsometry, Langmuir 17 (2001) 7529–7534.
[7] C. Lheveder, S. Hénon, J. Meunier, Brewster angle microscopy, in: A. Bazskin, W. Norde (Eds.), Physical Chemistry of Biological Interfaces, Marcel Dekker, Inc., New York 2000, pp. 559–576.
[8] D. Ducharme, J.J. Max, C. Salesse, R.M. Leblanc, Ellipsometric study of the physical states of phosphatidylcholines at the air-water interface, J. Phys. Chem. 94 (1990) 1925–1932.
[9] V. Tsukanova, C. Salesse, On the nature of conformational transition in poly(ethylene glycol) chains grafted onto phospholipid monolayers, J. Phys. Chem. B 108 (2004) 10754–10764.
[10] M.L. Fanani, B. Maggio, Liquid-liquid domain miscibility driven by composition and domain thickness mismatch in ternary lipid monolayers, J. Phys. Chem. B 115 (2011) 41–49.
[11] F. Dupuy, B. Maggio, The hydrophobic mismatch determines the miscibility of ceramides in lipid monolayers, Chem. Phys. Lipids 165 (2012) 615–629.
[12] S. Lafont, H. Rapaport, G.J. Sömjen, A. Renault, P.B. Howes, K. Kjaer, J. Als-Nielsen, L. Leiserowitz, M. Lahav, Monitoring the nucleation of crystalline films of cholesterol on water and in the presence of phospholipid, J. Phys. Chem. B 102 (1998) 761–765.
[13] R.G. Oliveira, M. Tanaka, B. Maggio, Many length scales surface fractality in monomolecular films of whole myelin lipids and proteins, J. Struct. Biol. 149 (2005) 158–169.
[14] A.A. Bischof, N. Wilke, Molecular determinants for the line tension of coexisting liquid phases in monolayers, Chem. Phys. Lipids 165 (2012) 737–744.
[15] K. Winsel, D. Honig, K. Lunkenheimer, K. Geggel, C. Witt, Quantitative Brewster angle microscopy of the surface film of human broncho-alveolar lavage fluid, Eur. Biophys. J. 32 (2003) 544–552.

[16] R.G. Oliveira, E. Schneck, S.S. Funari, M. Tanaka, B. Maggio, Equivalent aqueous phase modulation of domain segregation in myelin monolayers and bilayer vesicles, Biophys. J. 99 (2010) 1500–1509.
[17] E. Schneck, T. Schubert, O.V. Konovalov, B.E. Quinn, T. Gutsmann, K. Brandenburg, R.G. Oliveira, D.A. Pink, M. Tanaka, Quantitative determination of ion distributions in bacterial lipopolysaccharide membranes by grazing-incidence X-ray fluorescence, Proc. Natl. Acad. Sci. U. S. A. 107 (2010) 9147–9151.
[18] M. Ardhammar, P. Lincoln, B. Norden, Invisible liposomes: refractive index matching with sucrose enables flow dichroism assessment of peptide orientation in lipid vesicle membrane, Proc. Natl. Acad. Sci. U. S. A. 99 (2002) 15313–15317.
[19] B.N. Khlebtsov, V.A. Khanadeev, N.G. Khlebtsov, Determination of the size, concentration, and refractive index of silica nanoparticles from turbidity spectra, Langmuir 24 (2008) 8964–8970.
[20] S. Hénon, J. Meunier, Microscope at the Brewster angle: direct observation of first-order phase transitions in monolayers, Rev. Sci. Instrum. 62 (1991) 936–939.
[21] R.G. Oliveira, R.O. Calderon, B. Maggio, Surface behavior of myelin monolayers, Biochim. Biophys. Acta 1370 (1998) 127–137.
[22] Y. Min, K. Kristiansen, J.M. Boggs, C. Husted, J.A. Zasadzinski, J. Israelachvili, Interaction forces and adhesion of supported myelin lipid bilayers modulated by myelin basic protein, Proc. Natl. Acad. Sci. U. S. A. 106 (2009) 3154–3159.
[23] L. Yurlova, N. Kahya, S. Aggarwal, H.J. Kaiser, S. Chiantia, M. Bakhti, Y. Pewzner-Jung, O. Ben-David, A.H. Futerman, B. Brugger, M. Simons, Self-segregation of myelin membrane lipids in model membranes, Biophys. J. 101 (2011) 2713–2720.
[24] C.M. Rosetti, B. Maggio, R.G. Oliveira, The self-organization of lipids and proteins of myelin at the membrane interface. Molecular factors underlying the microheterogeneity of domain segregation, Biochim. Biophys. Acta 1778 (2008) 1665–1675.
[25] H. Inouye, J. Karthigasan, D.A. Kirschner, Membrane structure in isolated and intact myelins, Biophys. J. 56 (1989) 129–137.
[26] H. Inouye, D.A. Kirschner, Myelin: a one-dimensional biological “crystal” for x-ray and neutron scattering, in: J. Sedzik, P. Riccio (Eds.), Molecules: Nucleation, Aggregation and Crystallization, Beyond Medical and Other Implications, World Scientific Publishing Co., New Jersey 2009, pp. 75–94.
[27] J.E. Haley, F.G. Samuels, R.W. Ledeen, Study of myelin purity in relation to axonal contaminants, Cell. Mol. Neurobiol. 1 (1981) 175–187.
[28] J. Folch, I. Ascoli, M. Lees, J.A. Meath, B.N. Le, Preparation of lipide extracts from brain tissue, J. Biol. Chem. 191 (1951) 833–841.
[29] M.B. Lees, J.D. Sakura, Preparation of proteolipids, Res. Methods Neurochem. (1978) 345–370.
[30] C.M. Rosetti, R.G. Oliveira, B. Maggio, The Folch-Lees proteolipid induces phase coexistence and transverse reorganization of lateral domains in myelin monolayers, Biochim. Biophys. Acta 1668 (2005) 75–86.
[31] R.G. Oliveira, E. Schneck, B.E. Quinn, O.V. Konovalov, K. Brandenburg, U. Seydel, T. Gill, C.B. Hanna, D.A. Pink, M. Tanaka, Physical mechanisms of bacterial survival revealed by combined grazing-incidence X-ray scattering and Monte Carlo simulation, C. R. Chim. 12 (2009) 209–217.
[32] C.E. Vieira, A.A. Gasperini, P.P. Freitas, R.G. Oliveira, L.P. Cavalcanti, Characterization of a Pt mirror to be used to deflect synchrotron radiation beam onto Langmuir monolayers, J. Synchrotron Radiat. 22 (2015) 859–861.
[33] Y. Dai, B. Lin, M. Meron, K. Kim, B. Leahy, O.G. Shpyrko, A comparative study of Langmuir surfactant films: grazing incidence x-ray off specular scattering vs. x-ray specular reflectivity, J. Appl. Phys. 110 (2011) 102213.
[34] K. Kjaer, Some simple ideas on X-ray reflection and grazing-incidence diffraction from thin surfactant films, Phys. B Condens. Matter 198 (1994) 100–109.
[35] F.O. Schmitt, R.S. Bear, The ultrastructure of the nerve axon sheath, Biol. Rev. 14 (1939) 27–50.
[36] C.A. Helm, P. Tippmann-Krayer, H. Mohwald, J. Als-Nielsen, K. Kjaer, Phases of phosphatidyl ethanolamine monolayers studied by synchrotron x-ray scattering, Biophys. J. 60 (1991) 1457–1476.
[37] D. Marsh, Comment on interpretation of mechanochemical properties of lipid bilayer vesicles from the equation of state or pressure-area measurement of the monolayer at the air-water or oil-water interface, Langmuir 22 (2006) 2916–2919 (discussion 2920-2912).
[38] S.-s. Feng, Reply to comment on interpretation of mechanochemical properties of lipid bilayer vesicles from the equation of state or pressure-area measurement of the monolayer at the air-water or oil-water interface, Langmuir 22 (2006) 2920–2922.
[39] J.F. Nagle, S. Tristram-Nagle, Lipid bilayer structure, Curr. Opin. Struct. Biol. 10 (2000) 474–480.
[40] N.P. Franks, V. Melchior, D.A. Kirshner, D.L. Caspar, Structure of myelin lipid bilayers. Changes during maturation, J. Mol. Biol. 155 (1982) 133–153.
[41] C. Roldan-Carmona, J.J. Giner-Casares, M. Perez-Morales, M.T. Martin-Romero, L. Camacho, Revisiting the Brewster Angle Microscopy: the relevance of the polar headgroup, Adv. Colloid Interf. Sci. 173 (2012) 12–22.
[42] D.F. Kienle, J.V. de Souza, E.B. Watkins, T.L. Kuhl, Thickness and refractive index of DPPC and DPPE monolayers by multiple-beam interferometry, Anal. Bioanal. Chem. 406 (2014) 4725–4733.
[43] R. Bacallao, S. Sohrab, C. Phillips, Guiding principles of specimen preservation for confocal fluorescence microscopy, in: J. Pawley (Ed.), Handbook of Biological Confocal Microscopy, Springer, New York, 2006.
[44] C.P. Wendell-Smith, P.L. Williams, Some structural characteristics of myelinated nerve fibres, Nature 182 (1958) 1608–1609.